OPEN

Neuropsychopharmacology (2013) 38, 1221–1233
© 2013 American College of Neuropsychopharmacology. All rights reserved 0893-133X/13
www.neuropsychopharmacology.org

GluN2B Antagonism Affects Interneurons and Leads to Immediate and Persistent Changes in Synaptic Plasticity, Oscillations, and Behavior

Jesse E Hanson[1], Martin Weber[1], William J Meilandt[1], Tiffany Wu[1], Tom Luu[1], Lunbin Deng[1], Mehrdad Shamloo[2], Morgan Sheng[1], Kimberly Scearce-Levie[1] and Qiang Zhou*[,1]

[1]Department of Neuroscience, Genentech, Inc., South San Francisco, CA, USA; [2]Stanford Behavioral and Functional Neuroscience Laboratory, Stanford, CA, USA

Although antagonists to GluN2B-containing *N*-methyl-D-aspartate receptors (NMDARs) have been widely considered to be neuroprotective under certain pathological conditions, their immediate and lasting impacts on synaptic, circuit, and cognitive functions are poorly understood. In hippocampal slices, we found that the GluN2B-selective antagonist Ro25-6981 (Ro25) reduced synaptic NMDAR responses and consequently neuronal output in a subpopulation of GABAergic interneurons, but not pyramidal neurons. Consistent with these effects, Ro25 reduced GABAergic responses in pyramidal neurons and hence could affect circuit functions by altering the excitation/inhibition balance in the brain. In slices from Ts65Dn mice, a Down syndrome model with excess inhibition and cognitive impairment, acutely applied Ro25-rescued long-term potentiation (LTP) and gamma oscillation deficits, whereas prolonged dosing induced persistent rescue of LTP. In contrast, Ro25 did not impact LTP in wild-type (wt) mice but reduced gamma oscillations both acutely and following prolonged treatment. Although acute Ro25 treatment impaired memory performance in wt mice, memory deficits in Ts65Dn mice were unchanged. Thus, GluN2B–NMDARs contribute to the excitation/inhibition balance via impacts on interneurons, and blocking GluN2B–NMDARs can alter functions that depend on this balance, including synaptic plasticity, gamma oscillations, and memory. That prolonged GluN2B antagonism leads to persistent changes in synaptic and circuit functions, and that the influence of GluN2B antagonism differs between wt and disease model mice, provide critical insight into the therapeutic potential and possible liabilities of GluN2B antagonists.

Neuropsychopharmacology (2013) **38,** 1221–1233; doi:10.1038/npp.2013.19; published online 6 February 2013

Keywords: GluN2B; interneuron; oscillation; LTP; memory; Down syndrome

INTRODUCTION

N-methyl-D-aspartate receptors (NMDARs) are heteromeric receptors consisting of two GluN1 subunits and two GluN2A-D subunits, which have essential functions in brain development, synaptic signaling, and neuroplasticity. In the forebrain, GluN2A and GluN2B are the predominantly expressed NR2 subunits (Watanabe *et al*, 1993). Selective antagonists of GluN2B-containing NMDARs have been pursued for treating a variety of neurological conditions (Chazot, 2004; Mony *et al*, 2009), including ischemic stroke (Kaufman *et al*, 2012; Liu *et al*, 2007), Huntington's disease (Milnerwood *et al*, 2010; Okamoto *et al*, 2009), and Parkinson's disease (Calon *et al*, 2003; Wessell *et al*, 2004). A rationale for this approach is that GluN2B-containing NMDARs are thought to be excessively activated in these indications and could thus be selectively inhibited to prevent the synapse loss and/or neuronal cell death observed in these indications. Moreover, selective inhibition of GluN2B-containing NMDARs could potentially avoid the known side effects of non-selective NMDAR antagonists (Chazot, 2004; Mony *et al*, 2009) because of their preferential presence at extrasynaptic but not synaptic regions on excitatory pyramidal neurons in adult brain (Harris and Pettit, 2007; Papouin *et al*, 2012; Tovar and Westbrook, 1999). However, aside from pathological activation, evidence from both genetic deletion of GluN2B and acute systemic administration of GluN2B antagonists suggest a physiological role for GluN2B receptors in the adult brain during memory function (Mathur *et al*, 2009; von Engelhardt *et al*, 2008). Furthermore, a significant portion of the excitatory drive to inhibitory interneurons is mediated by NMDARs (Lei and McBain, 2002; Wang and Gao, 2009), and GluN2B subunits are expressed in GABAergic interneurons (Lei and McBain, 2002; Porter *et al*, 1998). Therefore, it needs to be tested whether GluN2B antagonists can significantly alter circuit functions by

*Correspondence: Dr Q Zhou, Department of Neuroscience, Genentech, Inc., 1 DNA Way, MS 230B, South San Francisco, CA 94080, USA, Tel: +1 650 467 7750, Fax: +1 650 225 4000, E-mail: zhou.qiang@gene.com
Received 5 October 2012; revised 21 December 2012; accepted 2 January 2013; accepted article preview online 22 January 2013

affecting NMDARs on interneurons. This is an important question not only for providing a deeper understanding of the contribution of NMDAR subunits to circuitry functions, but also for critically evaluating the therapeutic potential of GluN2B antagonists. Any possible benefits of blocking pathologically activated extrasynaptic GluN2B receptors would need to be carefully weighed against any alterations to the physiological functions of neural circuitry.

To address this, we studied the effects of the GluN2B-selective antagonist Ro25-6981 (Ro25; Fischer *et al*, 1997) on interneuron excitation, neural circuitry functions, and cognitive behavior, after either acute treatment or prolonged dosing, in both wild-type (wt) mice and the Ts65Dn mouse model of Down syndrome that features excess inhibition and cognitive impairment (Braudeau *et al*, 2011; Chakrabarti *et al*, 2010; Costa and Grybko, 2005; Fernandez *et al*, 2007; Kleschevnikov *et al*, 2012, 2004; Perez-Cremades *et al*, 2010; Rueda *et al*, 2008). We found that Ro25 disinhibited hippocampal circuitry by reducing excitatory drive to a subpopulation of hippocampal interneurons. *In vitro* application of Ro25 rescued deficits in long-term potentiation (LTP) and gamma oscillations in Ts65Dn Down syndrome model mice. Although this *in vitro* rescue did not translate into improvement of memory function in the Down syndrome mice, circuit function and memory in wt mice were disrupted. These results demonstrate novel physiological roles for GluN2B–NMDARs in interneurons and neural circuitry, and have broad implications for considering GluN2B antagonists as therapeutics.

MATERIALS AND METHODS

Animals

Three- to six-month-old male segmental trisomy 16 (Ts65Dn) mice and wt littermate controls were obtained from Jackson Labs (B6EiC3Sn a/A-Ts(1716)65Dn number 001924) or bred at Genentech. Some experiments, including the behavioral studies, used a related strain virtually identical to the original, but bred to not carry the recessive retinal degeneration mutation, $Pde6b^{rd1}$, (B6EiC3Sn.BLiA-Ts(1716)65Dn/DnJ number 005252; Costa *et al*, 2010). GABAergic interneurons were selectively targeted using 3-month-old GAD67-GFP knockin mice (Tamamaki *et al*, 2003). All animal studies were approved by the Genentech IUCAC, and conducted in accordance with the NIH Guide for the Care and Use of Laboratory Animals.

Drugs

Brain-slice experiments used the following: 50 nM NVP-AAM077 tetrasodium hydrate (NVP) and 3 μM Ro25 maleate from Santai Labs (China), 50 μM D-(-)-2-amino-5-phosphonopentanoic acid (AP5), 10 μM NBQX disodium salt, 100 μM picrotoxin (PTX), and 1 μM tetrodotoxin citrate from Tocris. For *in vivo* injection, Ro25 was formulated in 0.5% cremophor EL in saline with brief milling, and was dosed i.p. in a volume of 10 ml/kg.

Brain Slices

Horizontal slices (400–500 μm) containing hippocampus were prepared with a vibrating sectioning system (Leica, Germany), and were recorded in oxygenated artificial cerebrospinal fluid (ACSF) containing (in mM) 127 NaCl, 2.5 KCl, 1.3 MgSO4, 2.5 CaCl2, 1.25 Na2HPO4, 25 NaHCO3, and 25 glucose. Slices were prepared in ice-cold oxygenated ACSF with the MgSO4 concentration elevated to 7 mM, NaCl replaced with 110 mM choline, and with 11.6 mM Na-ascorbate and 3.1 mM Na-pyruvate.

Field Recordings

EPSPs and population spikes (PSs) were measured from the stratum radiatum (s. radiatum) and stratum pyramidale (s. pyramidale) regions of CA1, respectively, in response to stimulation of Schaffer collateral inputs. NMDAR EPSPs were measured with the Mg^{2+} concentration in the ACSF reduced to 0.5 mM and in the presence of PTX and NBQX. LTP was induced under conditions with intact inhibition using 1, 2, or 3 bouts of theta burst stimulation (TBS) separated by 20 s, each consisting of 5 pulses at 100 Hz repeated 10 times at 200-ms intervals. Tetanus-induced oscillations were recorded in the s. pyramidale following 200 ms of 100 Hz stimulation to the nearby region of s. radiatum proximal to the recording site. Gamma oscillations were analyzed after bandpass filtering at 30–200 Hz (8 pole Bessel). Spectrograms were generated with Matlab, and total power was calculated as the sum of power at all frequencies and all time points during the 1 s following stimulation. Ro25 was applied to brain slices for 20 min before assay of LTP or gamma oscillations. Oscillation power and EPSP magnitude during maximal stimulation were analyzed by two-factor ANOVAs, with genotype and drug treatment as the factors. The steady-state LTP responses following 1, 2, or 3 bouts of TBS were analyzed by three-factor ANOVAs with genotype, drug treatment, and number of TBS bouts as the factors. Pre-planned comparisons were performed using a Student's *t*-test to test specific hypotheses of deficits in Ts65Dn mice, Ro25 rescue of Ts65Dn deficits, and Ro25 alteration of wt function.

Whole-Cell Recordings

For current clamp recordings, internal solution consisted of (in mM) 120 K-gluconate, 20 KCl, 0.5 EGTA, 10 HEPES, 2.5 MgCl2, 4 Na2ATP, 0.3 NA3GTP, and 10 phosphocreatine. For voltage-clamp recordings, K-gluconate and KCl were replaced with Cs-methanesulfonate and CsCl, respectively, and 5 mM QX-314 bromide was added. Evoked EPSPs were measured at resting potentials that were subthreshold to action potential generation in response to single stimulations, and evoked EPSCs were measured at a holding potential of −70 mV. NMDAR EPSCs were measured at −70 mV in 0.5 mM Mg^{2+}, NBQX, and PTX. Significance of differences between the means was assessed using a Student's *t*-test.

Y-Maze

Individual mice were placed into a Y-maze and were allowed to explore the maze for 6 min. The number of arm entries and the sequence of arms entered was recorded by an observer unaware of either genotype or drug treatment. Non-performers with less than 10 arm entries throughout

the entire 6 min observation period were excluded from the analysis. A correct alternation was scored when a sequence of three consecutive arm entries (a triplet) included entries into all three arms of the maze. Percent alternations were calculated as $100 \times$ (number of correct alternations)/(total number of arm entires -2). Percent alternations and number of arm entries were analyzed by two-factor ANOVAs, with genotype and drug treatment as the between-subjects factors. ANOVAs were followed by Student's *t*-test when only two groups were compared.

Barnes Maze. The Barnes maze is a spatial memory test that utilizes the animals' tendency to escape from a brightly lit open environment into a quiet, dark escape tunnel. Mice were first familiarized with the maze, which consists of a circular table, 91 cm in diameter with 20 holes (5 cm diameter) equally spaced around the perimeter of the maze. Training consisted of allowing the mouse to freely explore the maze for up to 3 min to locate the target hole (in a new location from pre-training). During these 3 min, the number of errors (wrong holes explored), distance traveled, and latency to enter target hole were recorded using Cleversys software (TopScan). Immediately after the mouse entered the escape box, the lights were dimmed and the mouse was allowed to stay in the tunnel for 10–20 s. Animals were run with an intertrial interval of 15 min. Training occurred over 3 consecutive days. Latency to enter target hole, distance traveled, velocity (m/s), and errors (total number of nose pokes into incorrect holes) were analyzed using a two-factorial MANOVA with repeated measures with genotype and drug treatment as between-subjects and training days as within-subject repeated measure.

RESULTS

Ro25 Selectively Reduces Synaptic NMDAR Responses in S. Radiatum Interneurons, Decreases Interneuron Spiking, and Reduces Inhibition of Pyramidal Neurons

We first examined the function of GluN2B–NMDARs on pyramidal neurons in the hippocampal CA1 region using field NMDA–EPSP recordings. Consistent with previous results (Harris and Pettit, 2007; Papouin *et al*, 2012), we found that bath application of the selective GluN2B antagonist Ro25 (3 μM) partially reduced isolated synaptic NMDAR responses in CA1 pyramidal neurons in slices from young (2 week) but not more mature (4 week) animals (Figure 1a). We were able to block extrasynaptic NMDAR responses in pyramidal neurons from mature animals using Ro25 (Supplementary Figure S1A), indicating a selective exclusion of Ro25-sensitive NMDARs from synapses on pyramidal neurons.

Next we compared the effects of Ro25 on isolated synaptic NMDAR currents in interneurons located in s. radiatum or s. pyramidale of CA1, and found that NMDAR EPSCs in s. radiatum, but not s. pyramidale interneurons, were reduced by Ro25 in slices from mature animals (Figure 1b). On the other hand, adding the GluN2A-prefering antagonist NVP-AAM077 (50 nM) in addition to Ro25 caused a substantial reduction in s. pyramidale interneuron EPSCs, but only a modest change in the blockade in s. radiatum interneurons compared with Ro25 alone (Figure 1b). Thus, in contrast to pyramidal neurons or pyramidale interneurons, significant functional GluN2B–NMDARs are present at synapses on s. radiatum interneurons in mature brain slices. These radiatum interneurons exhibited regular firing characteristics in response to injection of depolarizing currents, in contrast to the fast spiking exhibited by the pyramidale interneurons (Supplementary Figure S2), and likely have a distinct role in circuit function. Using current clamp recordings, we found that Ro25 application reduced evoked EPSP area and spiking elicited by suprathreshold synaptic stimulation in radiatum, but not pyramidale interneurons (Figure 1c). To test if reduced spiking in interneurons could result in reduced inhibition of pyramidal neurons, we measured IPSCs in pyramidal neurons before and after Ro25 application. In these experiments, we used repetitive stimulation to resemble the activity patterns seen under physiologically relevant conditions, such as induction of synaptic plasticity and network oscillations. We observed a significant reduction of IPSCs amplitude during the first stimulus, and the profile of response amplitudes during repetitive stimulation was changed from facilitating to depressing in the presence of Ro25 (Figure 1d).

The above results raised the possibility that GluN2B antagonists could be useful to reduce excessive interneuron function observed in certain disease models. One such mouse model is the Ts65Dn model of Down syndrome, which exhibits increased interneuron production and inhibitory function (Braudeau *et al*, 2011; Chakrabarti *et al*, 2010; Costa and Grybko, 2005; Fernandez *et al*, 2007; Kleschevnikov *et al*, 2012, 2004; Perez-Cremades *et al*, 2010; Rueda *et al*, 2008). To test if inhibition is excessive in CA1 of Ts65Dn mice, we measured the ratio of inhibition to excitation, using stimulation that evoked similar amplitude EPSCs in both Ts65Dn and wt mice. A significant increase in the inhibition/excitation ratio was seen in Ts65Dn mice compared with wt mice (Figure 1e). To test if Ro25 could reduce the excitatory inputs to interneurons in Ts65Dn mice, we repeated the measurements of evoked EPSPs and synaptically driven interneuron spiking in Ts65Dn mice in the absence and presence of Ro25 (Figure 1f), and observed a reduction in EPSP area and synaptically driven spiking activity in s. radiatum but not s. pyramidale interneurons (Figure 1g). The magnitude of reduction was similar between Ts65Dn and wt mice. In addition, we observed that Ro25 could also effectively reduce evoked IPSCs of pyramidal neurons during repetitive stimulation in Ts65Dn mice (Figure 1h). At the same time, synaptic NMDAR responses in pyramidal neurons from adult mice were insensitive to Ro25 in both Ts65Dn and wt mice (Supplementary Figure S1B), indicating that the main target of Ro25 is likely to be glutamatergic synapses onto interneurons, but not pyramidal neurons in both wt and Ts65Dn mice.

Acute Application of Ro25 Rescues LTP Deficit in Hippocampal Slices from Ts65Dn Mice

LTP is impaired in Ts65Dn mice, and inhibiting $GABA_A$Rs can restore LTP in hippocampal slices (Costa and Grybko, 2005; Kleschevnikov *et al*, 2004). As GluN2B antagonism can reduce GABAergic responses in pyramidal neurons, it is

possible that GluN2B antagonist could counteract the excessive inhibition in Ts65Dn mice and restore LTP. We measured LTP following 1, 2, and 3 bouts of TBS in hippocampal slices from adult (3 month) wt and Ts65Dn mice. This protocol resulted in robust LTP in wt slices, but much reduced LTP in slices from Ts65Dn mice (Figure 2c and e). Acute bath application of Ro25 did not significantly affect LTP in wt slices, but restored LTP in Ts65Dn mice to a level similar to wt slices (Figure 2c and e). In addition to LTP of EPSPs, a similar rescue of deficits in population spike (PS) LTP was also seen in Ts65Dn mice in the presence of Ro25 (Figure 2d and f). Although this rescue of LTP is consistent with disinhibition by Ro25 in Ts65dn mice, it is also possible that Ro25 could cause an interneuron-independent impact on LTP. Therefore, we repeated the LTP experiments in the presence of the $GABA_AR$ antagonist, PTX, to test if Ro25 could have an effect on LTP in the absence of fast inhibitory synaptic transmission. Under these conditions, Ro25 had no impact on LTP (Figure 3). As these results suggest reduced inhibition has a critical role in the rescue of LTP deficit in the Ts65Dn mice, we would expect that the impact of Ro25 occurs during LTP induction. To examine this, we analyzed spiking activity during the TBS used to induce LTP. Although spiking (as measured by PS area) was relatively sustained during TBS in wt mice, the ability to sustain spiking during TBS was significantly diminished in Ts65Dn mice, but rescued in the presence of Ro25 (Supplementary Figure S3). Consistent with this excitation deficit and rescue in Ts65dn mice during LTP induction being mediated by inhibition, the deficit disappeared, and the benefit of Ro25 was occluded in the presence of PTX (Supplementary Figure S3). Interestingly, although total spiking (PS area) was sustained in wt mice regardless of Ro25 application, the apparent synchrony of spiking across the population of postsynaptic neurons (inferred from PS amplitude) was reduced by Ro25 application, an effect that was also occluded when inhibition was blocked (Supplementary

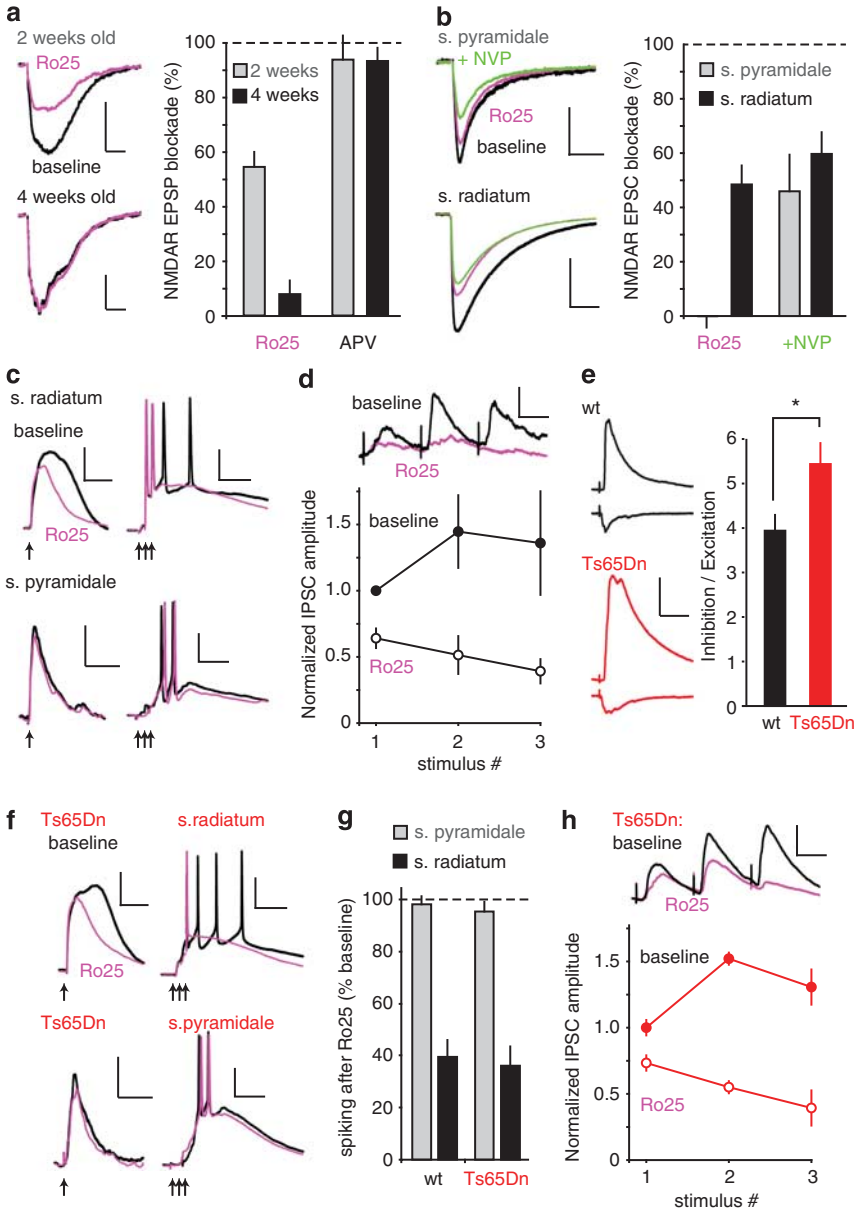

Figure S3). These results suggest that it is the total level of inhibition rather than the specific patterns of inhibition that influence LTP induction with this protocol.

Acute Application of Ro25 Rescues *In Vitro* Gamma Oscillation Deficits in Ts65Dn Mice but Impairs Gamma Oscillations in wt Mice

In addition to LTP, the balance between excitation and inhibition can also affect other network functions, such as the generation of synchronous oscillations. We induced oscillations in CA1 of hippocampal slices using tetanic stimulation, a phenomenon that depends on the activation of both excitatory and inhibitory synapses (Bracci *et al*, 1999; Vreugdenhil *et al*, 2005). Gamma oscillation power in slices from Ts65Dn mice was significantly reduced compared with wt mice (Figure 4). Acute Ro25 application restored oscillation power in slices from Ts65Dn mice, but significantly reduced oscillation power in slices from wt mice (Figure 4). Interestingly, the frequency profile and time course of oscillations were not affected by GluN2B antagonism in either genotype (Supplementary Figure S4). These results demonstrate that the acute circuit impacts of GluN2B antagonism extend beyond plasticity induction.

Prolonged Dosing with Ro25 Persistently Restores Synaptic Plasticity in Ts65Dn Mice

Previous work demonstrated that prolonged treatment (2 weeks) with $GABA_AR$ antagonists, which reduce inhibition, rescued deficits in cognitive function and LTP in Ts65Dn mice (Fernandez *et al*, 2007). Surprisingly, these improvements persisted for weeks even after dosing was discontinued, indicating lasting modification of circuit function. Therefore, we tested whether prolonged dosing with Ro25 could result in a lasting improvement of LTP in Ts65Dn mice, which could be detected after drug washout. In these experiments, mice were injected daily for 2 weeks with 50 mg/kg Ro25, a dose that achieves relevant brain exposure, with peak unbound brain levels reaching $0.958 \pm 0.126\,\mu M$ ($n = 3$ mice) immediately after injection and remaining above the IC_{50} of recombinant GluN2B–NMDARs (Fischer *et al*, 1997) for hours ($0.005 \pm 0.003\,\mu M$ at 6 h post injection). After 2 weeks of dosing, mice were allowed to recover for 2–4.5 weeks with no drug treatment before LTP was assessed (Figure 5a). Although this treatment regimen did not alter LTP in wt mice, it significantly improved LTP in Ts65Dn mice such that LTP was indistinguishable from wt mice (Figure 5b and d). Similarly, although PS LTP was unaltered in treated wt mice, deficits in PS LTP were significantly improved in treated Ts65Dn mice, resulting in partial restoration to wt levels (Figure 5c and e).

Prolonged Dosing with Ro25 Persistently Impairs *In Vitro* Gamma Oscillations and Increases Excitatory Synaptic Transmission in wt Mice

The persistent rescue of LTP in Ts65Dn mice indicates remodeling of circuit function following prolonged Ro25

Figure 1 Ro25-6981 (Ro25) selectively reduces synaptic *N*-methyl-D-aspartate receptor (NMDAR) responses and excitation-driven spiking in CA1 stratum radiatum (s. radiatum) interneurons and reduces inhibition of pyramidal neurons. (a) Representative pyramidal neuron field NMDAR–EPSP traces recorded before and after application of 3 μM Ro25 to slices from 2- and 4-week-old animals (scale bars: 0.25 mV/20 ms). Bar graph represents the mean ± SEM of the NMDA–EPSP area blocked by either 3 μM Ro25 or 50 μM 2-amino-5-phosphonopentanoic acid (APV; to verify the NMDAR-dependence of the EPSPs). Ro25 blockade was 54.4 ± 8.8% in 2-week-old and 7.8 ± 4.8% in 4-week-old animals ($n = 4$/age group, $p < 0.01$). APV blockade was 93.2 ± 5.2% in 2-week-old and 93.7 ± 2.2% in 4-week-old animals ($n = 4$/age group). (b) GAD67-GFP mice were used to examine synaptic NMDAR currents in stratum pyramidale (s. pyramidale) and s. radiatum GABAergic (GAD-67-positive) interneurons from mature mice. Example traces are shown for each type of interneuron before and after addition of Ro25 alone, or after addition of Ro25 and the GluN2A-preferring antagonist NVP-AAM077 tetrasodium hydrate (NVP; scale bars: s. pyramidale 40 pA/50 ms, s. radiatum 200 pA/100 ms). Bar graph shows the % blockade of the baseline EPSC area (mean ± SEM). NMDA EPSCs in s. pyramidale interneurons were not blocked by Ro25 alone (0.0 ± 4.2%, $n = 9$), but were significantly blocked when NVP was added in addition to Ro25 (46.0 ± 13.5%, $n = 9$), whereas NMDA EPSCs in s. radiatum interneurons were significantly blocked by Ro25 alone (48.5 ± 7.0%, $n = 7$). (c) Ro25 reduces EPSPs and synaptically driven spiking in s. radiatum, but not s. pyramidale interneurons. S. radiatum EPSP area in response to a single synaptic stimulation (arrow) was decreased following Ro25 application (scale bars: 10 mV/100 ms). When triple synaptic stimulations (100 Hz, arrows) were used to drive s. radiatum interneurons to fire multiple spikes, Ro25 application resulted in a reduction of spike number (scale bars: 20 mV/100 ms). S. pyramidale interneuron EPSPs (scale bars: 5 mV/100 ms) and evoked spiking (scale bars: 20 mV/50 ms) were not affected by Ro25 application. (d) The effects of Ro25 on inhibition in pyramidal neurons were assessed during repetitive stimulation. Example averaged traces are shown during baseline stimulation and following Ro25 wash on (scale bars: 25 pA/50 ms). Graphs show the IPSC amplitudes for each of the three stimuli normalized to the first response in the baseline condition. Solid circles show baseline IPSCs, and open circles show IPSCs in the presence of Ro25. Ro25 significantly reduced the amplitude of the first IPSC ($p < 0.05$, $n = 6$), and also had a pronounced effect on the profiles of subsequent responses. (e) The level of inhibition was assessed in pyramidal neurons from Ts65dn and wild-type (wt) slices by adjusting the stimulus intensity to evoke an EPSC of approximately 90 pA measured at −80 mV (wt = 91.0 ± 10.7, $n = 10$; Ts65Dn = 89.2 ± 12.1, $n = 11$), and IPSCs were then measured at 0 mV, using the same stimulus intensity. Example of EPSCs and IPSCs are shown for wt and Ts65Dn mice (scale bars: 200 pA and 50 ms, respectively). Bar graph shows the ratio of inhibition to excitation (IPSC amplitude divided by EPSC amplitude) in each genotype. Ts65Dn mice had a significantly higher level of inhibition than wt mice ($p < 0.05$, $n = 10,11$). (f) Ro25 reduces EPSPs and synaptically driven spiking in s. radiatum but not s. pyramidale interneurons in Ts65Dn mice. S. radiatum EPSP area in response to a single synaptic stimulation (arrow) was decreased following Ro25 application (scale bars: 10 mV/100 ms). When triple synaptic stimulations (100 Hz, arrows) were used to drive s. radiatum interneurons to fire multiple spikes, Ro25 application resulted in a reduction of spike number (scale bars: 20 mV/100 ms). S. pyramidale interneuron EPSPs (scale bars: 5 mV/100 ms) and evoked spiking (scale bars: 20 mV/50 ms) were not affected by Ro25 application. (g) Quantification of the % of baseline spiking remaining after Ro25 wash on in wt and Ts65Dn mice. After application of Ro25, s. radiatum interneuron spiking was 39.6 ± 6.3% of baseline in wt, and 36.1 ± 7.4% of baseline in Ts65Dn interneurons ($n = 4,4$), and s. pyramidale interneuron spiking was 98.1 ± 3.1% of baseline in wt, and 95.2 ± 3.7% of baseline in Ts65Dn interneurons ($n = 4,4$). (h) The effects of Ro25 on inhibition during repetitive stimulation in Ts65Dn slices. Example averaged traces are shown during baseline stimulation and following Ro25 wash on (scale bars: 50 pA/50 ms). Graphs show the IPSC amplitudes for each of the three stimuli normalized to the first response in the baseline condition. Solid circles show baseline IPSCs, and open circles show IPSCs in the presence of Ro25. Ro25 significantly reduced the amplitude of the first IPSC ($p < 0.05$, $n = 4$), and also had a pronounced effect on the profiles of subsequent responses. All data is shown as mean ± SEM, $^*p < 0.05$.

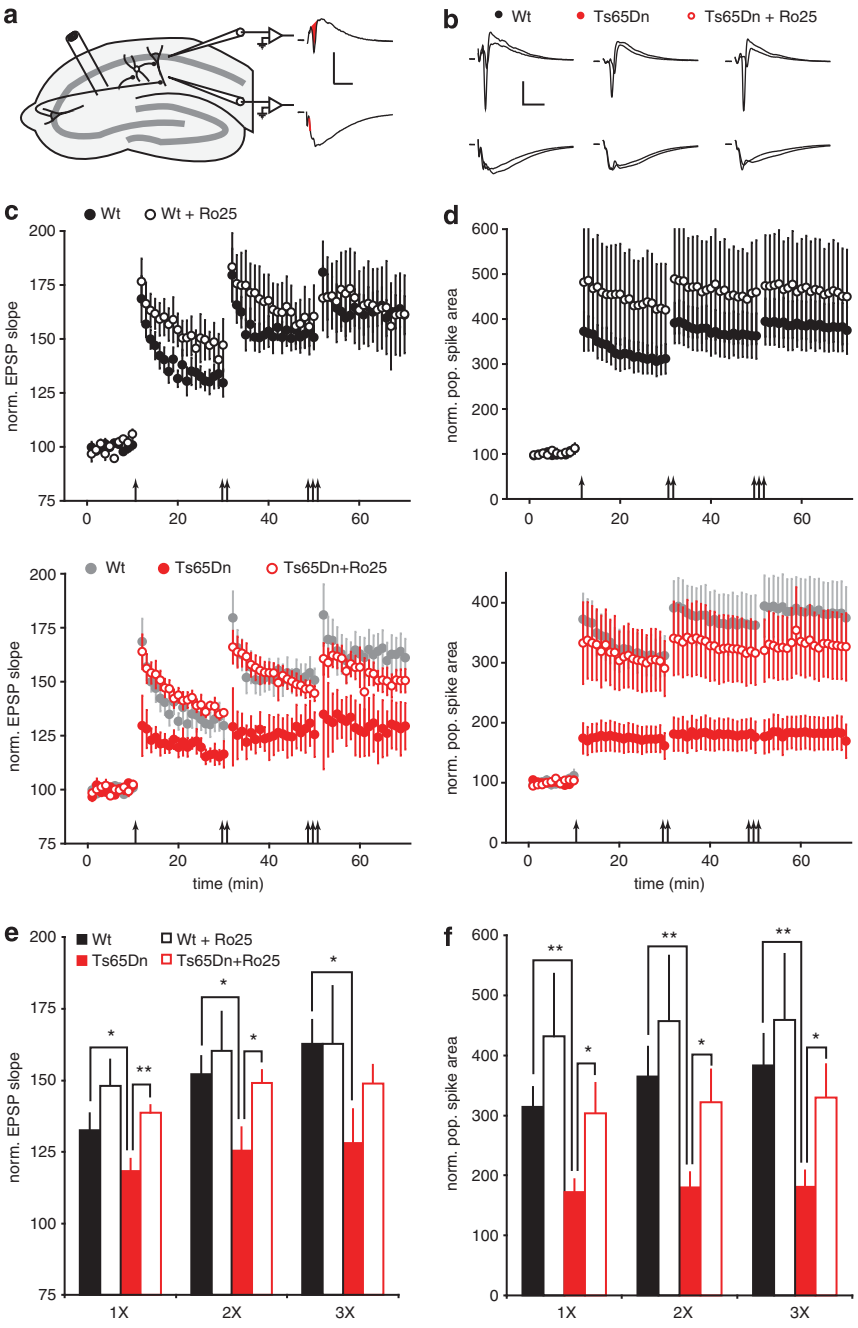

Figure 2 Ro25-6981 (Ro25) application rescues long-term potentiation (LTP) deficits in slices from Ts65Dn mice. (a) Recording and stimulation configuration. LTP was measured in the CA1 region of the hippocampus in response to Schaffer collateral stimulation under conditions that include activation of interneurons. EPSP initial slope was measured from recordings in stratum radiatum (s. radiatum; bottom, red line), and populaion spike (PS) area was measured from recordings in stratum pyramidale (s. pyramidale; top, red area, scale bars: 0.5 mV/10 ms). (b) Representative EPSP (bottom) and PS (top) traces from wild-type (wt) and Ts65Dn mice in the presence of vehicle and Ts65Dn mice in the presence of Ro25 (scale bars: 0.5 mV/10 ms). (c) EPSP LTP in slices from mice treated with vehicle or Ro25 in response to sequential bouts of 1, 2, or 3 × theta burst stimulation (TBS) is shown. The upper graph shows LTP in wt mice ($n = 6, 7$), and the lower graph shows LTP in Ts65Dn mice ($n = 6, 7$), with wt vehicle data replotted in gray for comparison. (d) PS LTP from the same experiments as in panel c is shown. (e) Binned EPSP LTP data from the last 10 min following 1, 2 or 3 × TBS are shown. There were significant effects of both genotype ($p < 0.05$) and treatment ($p < 0.05$). Planned comparisons showed that EPSP LTP was significantly reduced in vehicle-treated Ts65Dn mice compared with wt mice (1 × TBS, $p < 0.05$; 2 × , $p < 0.05$; 3 × , $p < 0.05$) and that Ro25 significantly enhanced EPSP LTP in Ts65Dn mice compared with vehicle (1 × , $p < 0.01$; 2 × , $p < 0.05$). (f) Binned PS LTP data are shown. There were significant effects of both genotype ($p < 0.01$) and treatment ($p < 0.05$). Planned comparisons showed that PS LTP was significantly reduced in vehicle-treated Ts65Dn mice compared with wt mice (1 × TBS, $p < 0.01$; 2 × , $p < 0.01$; 3 × , $p < 0.01$) and that Ro25 significantly enhanced PS LTP in Ts65Dn mice compared with vehicle (1 × , $p < 0.05$; 2 × , $p < 0.05$; 3 × , $p < 0.05$). All data in this figure are shown as mean ± SEM, *$p < 0.05$, **$p < 0.01$.

dosing. Therefore, we tested *in vitro* gamma oscillations in slices after the same dosing and washout regimen. Prolonged Ro25 dosing resulted in an impairment of oscillation power in wt mice, but did not affect oscillations in Ts65Dn mice (Figure 6a and b). No changes in the oscillation frequency profile and time course were observed

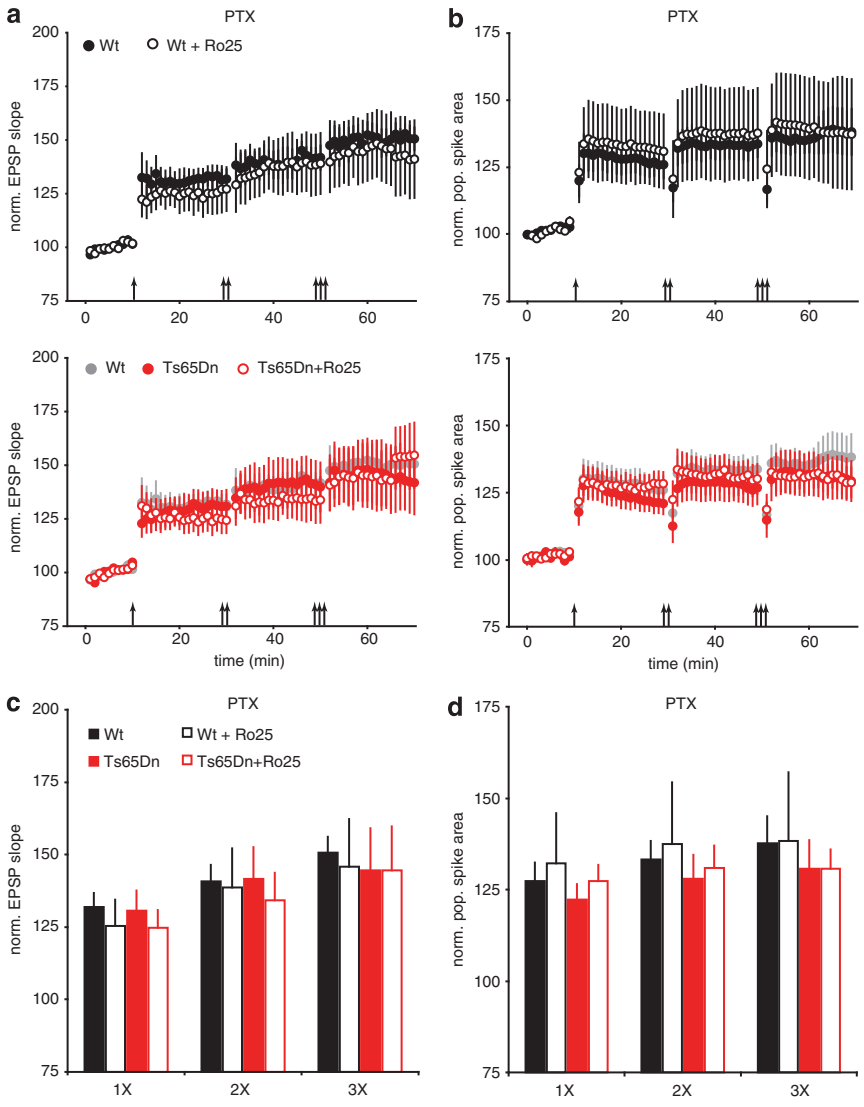

Figure 3 Ro25-6981 (Ro25) has no impact on long-term potentiation (LTP) in the presence of picrotoxin (PTX). (a) EPSP LTP in slices from mice treated with vehicle or Ro25 in response to sequential bouts of 1, 2, or 3 × theta burst stimulation (TBS) is shown. The upper graph shows LTP in wild-type (wt) mice ($n = 6, 7$), and the lower graph shows LTP in Ts65Dn mice ($n = 6, 7$), with wt vehicle data replotted in gray for comparison. (b) Population spike (PS) LTP from the same experiments as in panel a is shown. (c) Binned EPSP LTP data from the last 10 min following 1, 2, or 3 × TBS in the presence of PTX is shown. There were no significant effects of genotype or treatment, and planned comparisons did not show any significant deficits in EPSP LTP in Ts65Dn mice or any effects of Ro25. (d) Binned PS LTP data in the presence of PTX is shown. There were no significant effects of genotype or treatment, and planned comparisons did not show any significant deficits in PS LTP in Ts65Dn mice or any effects of Ro25.

with treatment in either genotype (Supplementary Figure S5). Although the reduction in gamma oscillation power in wt mice resembles the effect of acute *in vitro* application of Ro25, the lack of impact on oscillations in Ts65Dn mice contrasts with the increased power with acute application, suggesting functional circuit changes following prolonged treatment do not simply mimic the acute impacts of Ro25.

Although conceivably the functional circuit alterations following prolonged dosing could simply be caused by changes in the NMDAR function, several observations argue against this possibility: (1) a similar reduction in gamma oscillation power was seen after complete blocking of NMDARs by the non-selective NMDAR antagonist 2-amino-5-phosphonopentanoic acid (APV) in slices from both vehicle-treated and Ro25-treated wt and Ts65Dn mice (Supplementary Figure S6A); (2) The extent of Ro25-induced inhibition of isolated synaptic NMDAR responses in radiatum interneurons was not altered in either genotype (Supplementary Figure S6B); (3) No significant changes in GluN1, GluN2A, or GluN2B protein levels were detected in hippocampi from either genotype (Supplementary Figure S6C). Together, these data suggest that the impairment of gamma oscillations in wt mice following prolonged dosing is unlikely to be caused by gross changes to the NMDAR expression or function.

Although the direct impacts of Ro25 are likely limited to synapses onto interneurons, persistent alterations to circuit function following prolonged Ro25 dosing could involve other parts of the circuitry. Therefore, we examined excitatory drive to CA1 pyramidal neurons following prolonged Ro25 dosing and washout, and observed

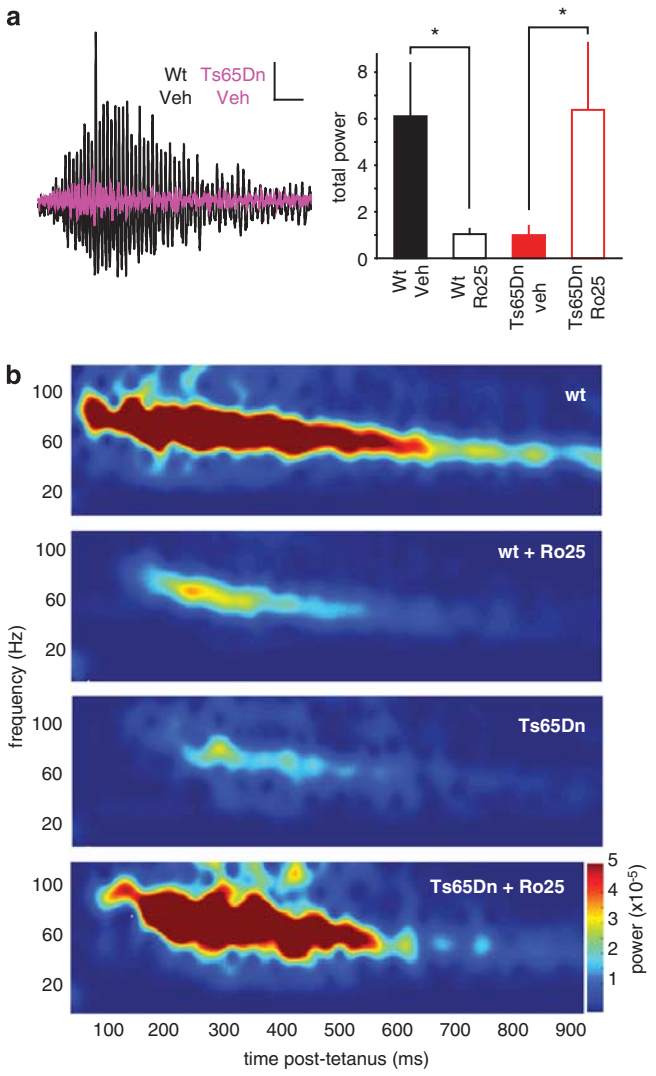

Figure 4 Ro25-6981 (Ro25) acutely impairs gamma oscillations *in vitro* in wild-type (wt) mice, but improves oscillations in Ts65dn mice. (a) Example traces showing tetanus-induced oscillations from vehicle-treated wt (black) and Ts65Dn slices (purple, scale bars: 0.1 mV/100 ms). The total gamma power in wt mice during the 1-s epoch following tetanization is shown as mean ± SEM, $*p<0.05$. There was a significant interaction between genotype and treatment ($p=0.01$), and planned comparisons showed that Ro25-treated wt slices had significantly less power than vehicle-treated wt slices ($p<0.05$), whereas Ro25-treated Ts65Dn slices had significantly more power than vehicle-treated Ts65Dn slices ($p<0.05$). (b) Average spectrograms from wt and Ts65Dn slices treated with Ro25 or vehicle ($n=10$ wt veh, 13 wt Ro25, 8 Ts65Dn veh, 11 Ts65Dn Ro25) show the differing levels of total power.

enhanced basal synaptic transmission and output spiking in wt mice, but not in Ts65Dn mice (Figure 6c–e). This selective increase in excitatory synaptic function was also present when synaptic inhibition was blocked with PTX (Supplementary Figure S7), indicating that the enhanced synaptic excitation is not secondary to alterations to synaptic inhibition. Thus, prolonged dosing with Ro25 can lead to lasting perturbation of the basal excitatory synaptic properties of neural networks in wt mice, which could potentially underlie the observed deficits in *in vitro* gamma oscillations.

Ro25 Dosing Differentially Affects Cognitive Behavior in Ts65Dn and wt Mice

To test whether the Ro25-induced alterations observed *in vitro* lead to changes in cognitive functions, we examined Y-maze performance in wt and Ts65Dn mice. Vehicle-treated Ts65Dn mice made significantly fewer alternations than wt mice in the Y-maze (Figure 7a). Although other processes such as novelty-seeking could impact this measure, reduced alternations in this assay are consistent with working memory impairment. Acute Ro25 injections (50 mg/kg) 1 h before the Y-maze assay resulted in a marked genotype-dependent effect on the alternations: Ts65Dn mice performed significantly better than wt mice (Figure 7a). This difference was caused by a significant impairment in the wt mice rather than an improvement in the Ts65Dn mice with Ro25. Furthermore, this effect was not due to altered activity levels by Ro25. Although Ts65Dn mice exhibited hyperactivity in general, there was no significant change in arm entries following Ro25 injection in wt or Ts65Dn mice (Figure 7a). This genotype-dependent effect on the Y-maze performance with Ro25 was replicated in a second study by an independent laboratory (SFBNL) using 10 or 50 mg/kg Ro25 (Supplementary Figure S8). These Y-maze results demonstrate a differential impact of acute Ro25 on wt *vs* Ts65Dn mice *in vivo*. On the other hand, prolonged Ro25 dosing did not affect the Y-maze performance of either genotype (Figure 7b). Prolonged treatment did affect cognitive behavior, however, as assessed with the Barnes maze, a distinct test of spatial memory in which Ts65Dn mice also show deficits (Figure 7c). In the Barnes maze, prolonged Ro25 treatment reduced performance in Ts65Dn mice but not in wt mice (Figure 7c), again emphasizing the genotype- and treatment regimen-dependent effects of Ro25. Overall, although cognitive impairment in the Ts65Dn mice was not rescued by GluN2B antagonism, these behavioral experiments provide *in vivo* confirmation of several of the major insights of the electrophysiological analysis as follows: (1) Ro25 has acute impacts; (2) prolonged Ro25 dosing induces lasting changes; and (3) both of these phenomena are genotype-dependent.

DISCUSSION

Although much previous work on GluN2B antagonists has focused on their neuroprotective roles in pathological situations, we have described novel impacts of GluN2B antagonism under normal physiological conditions via contribution to excitatory drive of interneurons.

Antagonizing GluN2B–NMDARs led to differential changes in LTP and gamma oscillations in wt *vs* Ts65Dn Down syndrome model mice. Acute GluN2B antagonism also led to impaired memory performance in wt mice without altering memory deficits in Ts65Dn mice. The importance of GluN2B–NMDARs to normal circuit function is further emphasized by the lasting changes to neural circuit function following prolonged antagonist dosing.

Cell-Type Specific Impacts of GluN2B Antagonism

We found that GluN2B antagonists inhibited synaptic NMDARs on s. radiatum interneurons but not excitatory

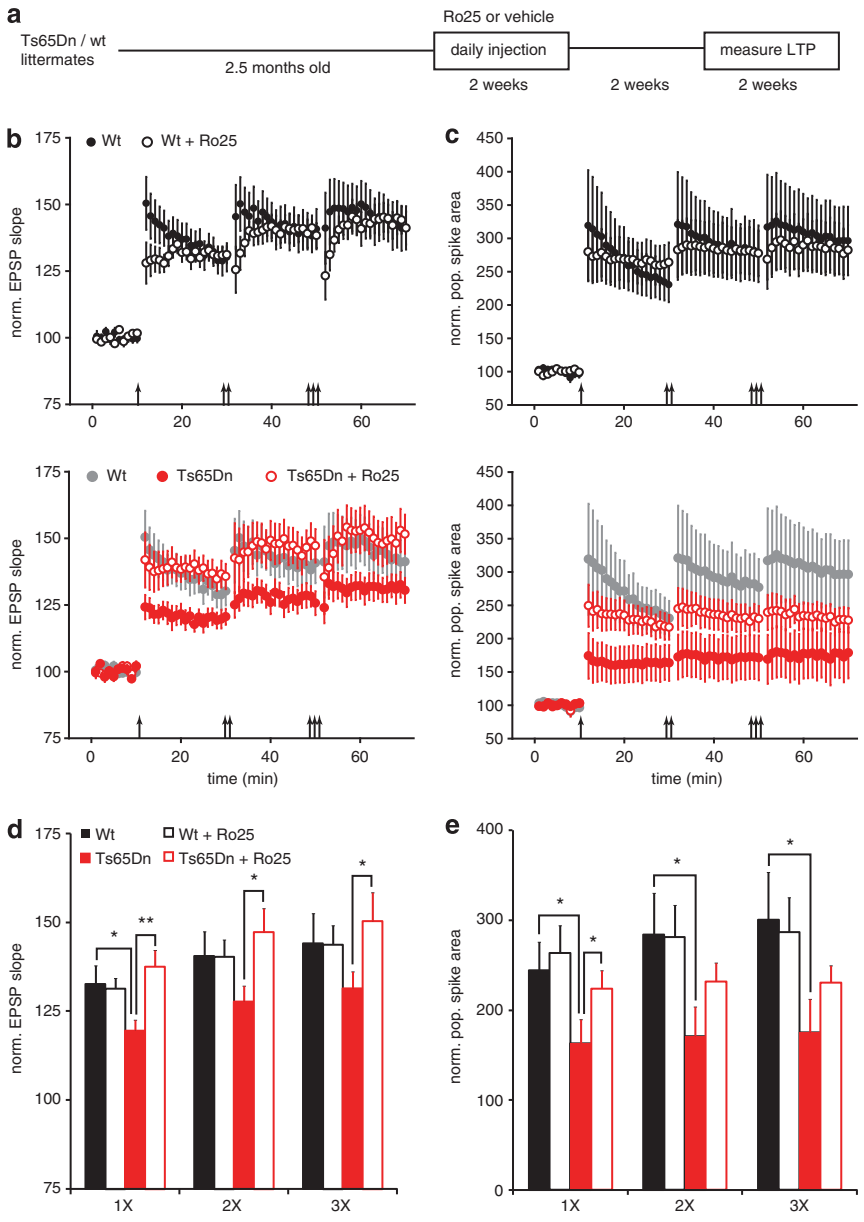

Figure 5 Prolonged Ro25-6981 (Ro25) dosing persistently rescues long-term potentiation (LTP) in Ts65Dn mice. (a) 2.5–3-month-old mice were injected with 50 mg/kg Ro25 or vehicle daily for 2 weeks, followed by at least a 2-week washout period before LTP was measured as in Figure 2 (over a period of 2.5 weeks). (b) EPSP LTP in slices from mice treated with vehicle or Ro25 in response to sequential bouts of 1, 2, or 3 × theta burst stimulation (TBS) is shown. The upper graph shows LTP in wild-type (wt) mice ($n = 16$, 12), and the lower graph shows LTP in Ts65Dn mice ($n = 11$, 14), with wt vehicle data replotted in gray for comparison. (c) Population spike (PS) LTP from the same experiments as in panel c is shown. (d) Binned EPSP LTP data from the last 10 min following 1, 2 or 3 × TBS is shown. There was a significant interaction between genotype and treatment ($p < 0.01$). Planned comparisons showed that LTP was significantly reduced in slices from vehicle-treated Ts65Dn mice compared with vehicle-treated wt mice (1 ×, $p < 0.05$), and that Ro25 treatment significantly enhanced LTP in Ts65Dn mice compared with vehicle (1 ×, $p < 0.01$; 2 ×, $p < 0.05$; 3 ×, $p < 0.05$). Wt vehicle data from panel b is in gray. All data in this figure is shown as mean ± SEM. (e) Binned PS LTP data is shown. There was a significant effect of genotype on PS LTP. Planned comparisons showed that PS LTP was significantly reduced in vehicle-treated Ts65Dn mice compared with wt mice (1 ×, $p < 0.01$; 2 ×, $p < 0.01$; 3 ×, $p < 0.01$) and that Ro25 significantly rescued PS LTP in Ts65Dn mice treated with Ro25 compared with vehicle (1 ×, $p < 0.05$). All data is shown as mean ± SEM, *$p < 0.05$, **$p < 0.01$.

pyramidal neurons or s. pyramidale interneurons. The lack of impact of GluN2B antagonists on pyramidal neurons is consistent with previous reports (Harris and Pettit, 2007; Papouin *et al*, 2012). As GluN2B antagonists have been shown to be more effective in inhibiting diheteromeric NMDARs (NR1/NR2B) than triheteromeric NMDARs (NR1/NR2A/NR2B), one possible explanation is that triheteromeric NMDARs constitute the main population of synaptic NMDARs on pyramidal neurons, whereas s. radiatum interneurons have a significant amount of synaptic diheteromeric GluN2B–NMDARs (see Supplementary Discussion SI).

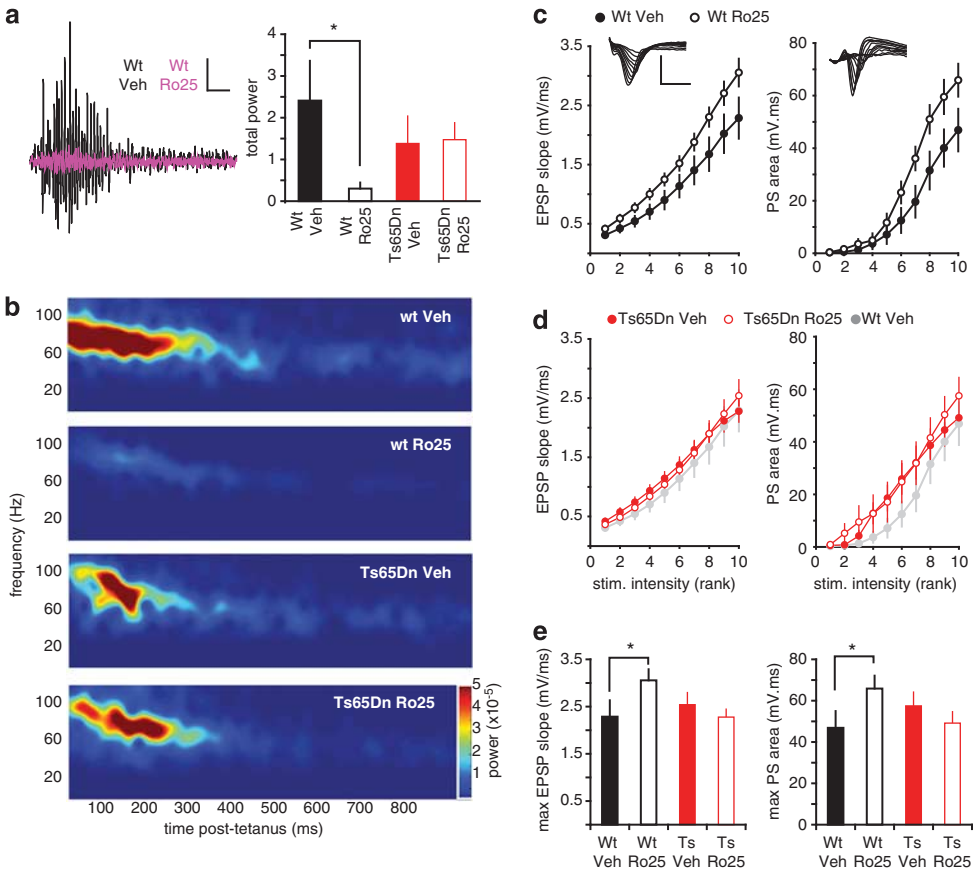

Figure 6 Prolonged Ro25-6981 (Ro25) dosing persistently impairs *in vitro* gamma oscillations and enhances excitation in wild-type (wt) mice. (a) Effects of prolonged Ro25 treatment on gamma oscillations. Example traces following tetanus-induced oscillations in vehicle-treated (black) and Ro25-treated wt mice (purple; scale bars: 0.1 mV/100 ms) are shown. Although there wasn't a significant interaction between genotype and treatment ($p = 0.096$), planned comparisons showed that oscillation power in slices from Ro25-treated wt mice was significantly lower than that from vehicle-treated wt mice ($p < 0.05$), whereas Ro25 treatment did not alter oscillation power in Ts65Dn mice. (b) Average spectrograms from recordings in wt and Ts65Dn mice treated with Ro25 ($n = 11$ wt veh, 8 wt Ro25, 12 Ts65Dn veh, 14 Ts65Dn Ro25), show greatly reduced power in Ro25-treated wt mice. (c) Measurement of excitatory synaptic strength. Stimulus intensity (logarithmically spaced) *vs* EPSP magnitude relationships are shown for wt mice treated with vehicle or Ro25 (left). Example EPSP recordings are inset (scale bars: 2 mV/50 ms). The right panel shows simultaneously measured population spike (PS) data ($n = 13$ vehicle, 14 Ro25; $p < 0.05$). (d) Stimulus intensity *vs* EPSP (left) and PS magnitude (right) relationships are shown for Ts65Dn mice treated with vehicle or Ro25 ($n = 13$ vehicle, 15 Ro25). Data from vehicle-treated wt mice from panel a is shown in gray for comparison. (e) Maximal EPSP and PS responses are plotted for all genotype and treatment groups under baseline conditions. There was a significant interaction between genotype and treatment for both EPSP and PS responses ($p < 0.05$), and planned comparisons showed that both EPSP and PS magnitudes were significantly greater in slices from Ro25-treated wt mice compared with vehicle-treated wt mice ($p < 0.05$). Slices from vehicle-treated Ts65Dn mice did not significantly differ from vehicle-treated wt slices, and Ro25 treatment did not significantly alter maximal EPSP or PS magnitude in slices from Ts65Dn mice compared with vehicle treatment. Data is shown as mean ± SEM, $^*p < 0.05$.

That GluN2B–NMDARs function is selective to s. radiatum *vs* s. pyramidale interneurons is consistent with the much longer time course of EPSPs in s. radiatum interneurons. These interneurons provide feed-forward inhibition of pyramidal neurons (Maccaferri and Dingledine, 2002) and have axonal projections that are associated with Schaffer collateral inputs to pyramidal neurons (Vida *et al*, 1998), and are thus positioned to regulate depolarization of pyramidal neurons during synaptic activation. Therefore, reduction of excitatory inputs to s. radiatum interneurons by GluN2B antagonism could affect the overall level of inhibition of pyramidal neurons, and thereby gate functions like synaptic plasticity. At the same time s. radiatum interneurons also provide inhibition to other interneuron types within CA1 (Chamberland and Topolnik, 2012), and could cause additional indirect impacts to circuit function when their activation is reduced by GluN2B antagonism.

GluN2B Antagonism Reduces Inhibition and Alters Circuit Function

We found that Ro25 reduced synaptic inhibition of pyramidal neurons and rescued LTP deficits in Ts65Dn mice that have excess inhibition. The rescue of LTP by Ro25 appears to be mediated via effects on inhibition, as Ro25's effects in Ts65Dn mice are occluded in the presence of the $GABA_AR$ blockers. We speculate that the gamma oscillation deficits that we report here for the first time could also be caused by excess inhibition in Ts65Dn mice, as they were also rescued by Ro25. Although we cannot exclude a role of extrasynaptic GluN2B-containing NMDARs in the circuit

level phenomena, the disinhibition achieved by the action of Ro25 at synaptic NMDARs on interneurons alone would be sufficient to explain the rescue of LTP and gamma oscillation in Ts65Dn mice. In wt slices, disinhibition likely leads to suboptimal function by shifting the balance between excitation and inhibition towards excessive excitation, and could underlie the reduction of wt gamma oscillation power with Ro25. Although we did not observe an impact of Ro25 on fast spiking interneurons, which directly control gamma oscillations (Sohal *et al*, 2009), our finding of altered oscillations with Ro25 is consistent with recent findings also demonstrating a contribution of GluN2B receptors to oscillations (Kocsis, 2012a; McNally *et al*, 2011), and suggests that s. radiatum interneurons could mediate this modulation.

In addition to acute impacts, we observed lasting impacts of prolonged dosing, which did not simply mimic the effects of acute application/dosing. Although acute GluN2B antagonism decreases inhibition, prolonged antagonism results in enhanced excitation in wt mice. This impact of prolonged dosing should cause a similar imbalance to circuit function and could account for the similar deficits in gamma oscillations in wt mice as seen with acute Ro25 application. We cannot exclude the possibility that the reported off-target effects of Ro25, such as impacts on monoamine neurotransmission (Keiser *et al*, 2009), could contribute to some of the phenotypes seen with chronic treatment. However, that the rescue of LTP in chronically treated Ts65Dn mice resembles the effects of a similar treatment regimen using $GABA_AR$ antagonists (Fernandez *et al*, 2007) and is consistent with prolonged disinhibition by Ro25 being responsible for inducing lasting functional alterations.

Implications for Therapeutic use of GluN2B Antagonists

Our results highlight that the effects of GluN2B antagonism vary depending on disease state, as differential effects on circuit function and behavior were consistently observed in Ts65Dn *vs* wt mice with both acute and prolonged Ro25 treatment. That the specific consequences of GluN2B antagonist treatment are determined by the state of brain circuitry is in agreement with an *in vivo* study showing sleep-state dependent effects of Ro25 on gamma activity (Kocsis, 2012b), and the differential impacts of Ro25 on gamma oscillations in wt brain slices induced by a tetanus (our study) *vs* kainate application (McNally *et al*, 2011). The

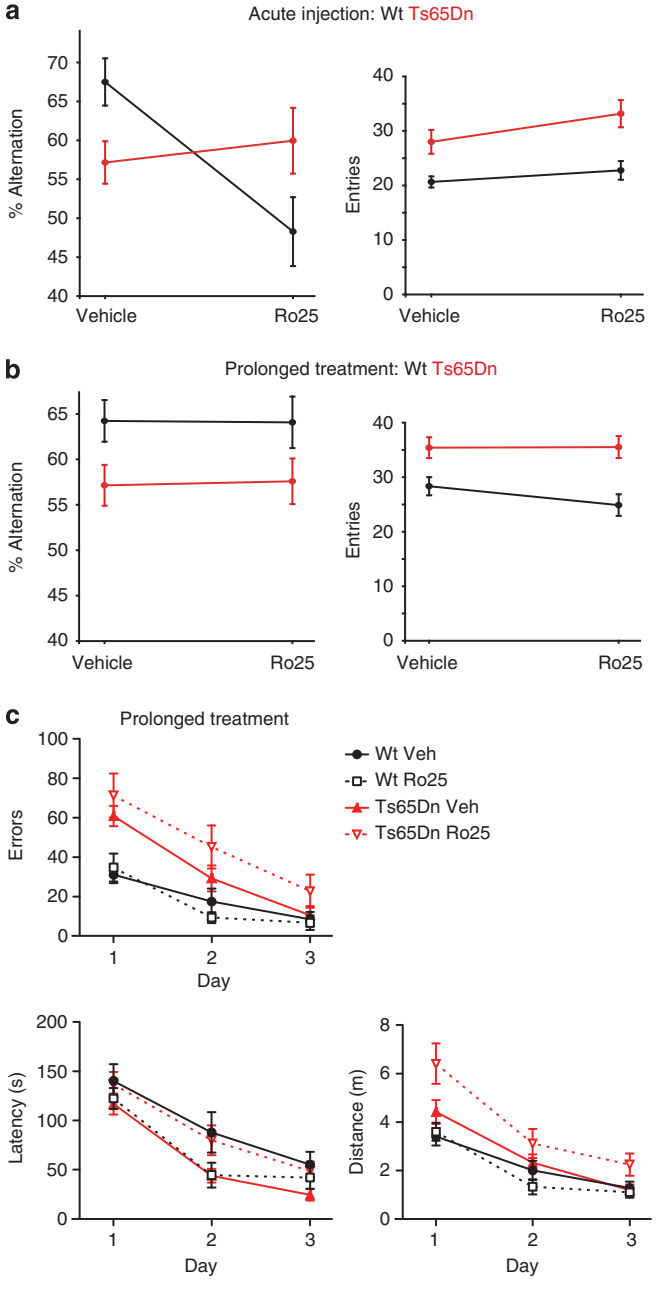

Figure 7 Ro25-6981 (Ro25) dosing differentially affects cognitive behaviors in wild-type (wt) and Ts65Dn mice, depending on dosing regimen (acute *vs* prolonged). (a) Y-maze alternations and entries are shown following acute Ro25 treatment. There was a significant genotype × treatment effect on the Y-maze alternations following acute Ro25 treatment ($p<0.005$; $n=14/12$ Ts65Dn and 14/13 wt vehicle/Ro25). Vehicle-treated Ts65Dn mice were impaired in percent alternations compared with wt mice ($p<0.05$), indicating a deficit in Ts65Dn mice. However, Ro25-treated wt mice exhibited significantly impaired alternations compared with Ro25-treated Ts65Dn mice ($p<0.05$). This was due to a significant impairment of alternations in Ro25-treated wt mice compared with vehicle-treated wt mice ($p<0.05$), and no significant effect of Ro25 treatment on Ts65Dn mice. Although there was an effect of genotype on arm entries ($p<0.0001$) reflecting increased activity of Ts65Dn mice, there were no genotype × treatment or treatment effects on arm entries. (b) Y-maze alternations and entries are shown following prolonged Ro25 dosing. There was an effect of genotype ($p<0.01$; $n=20/19$ Ts65Dn and 20/18 wt vehicle/ Ro25), with the Ts65Dn mice showing impaired alternations compared with wt mice, but there were no treatment or genotype × treatment effects on alternations. There was also an effect of genotype on arm entries ($p<0.0001$), with more arm entries in Ts65Dn mice than in wt mice, but there were no treatment or genotype × treatment effects on entries. (c) Barnes maze performance across 3 days of training is shown following prolonged Ro25 dosing. All groups learned the task with improved latency, distance, and error levels across days of training ($p<0.0001$; $n=10/9$ Ts65Dn and 9/8 wt vehicle/Ro25), but Ts65Dn mice showed significant impairments in both distance ($p<0.01$) and errors ($p<0.0001$) compared with wt mice. Significant genotype × treatment effects were observed for latency ($p<0.05$) and distance ($p<0.05$). This reflected a significantly increased latency ($p<0.05$) and distance ($p<0.05$) in Ro25-treated Ts65Dn mice compared with vehicle-treated Ts65Dn mice, whereas Ro25 treatment did not significantly affect wt mice. All data is shown as mean ± SEM.

results of our study suggest that a key aspect of the brain state that determines the effects of GluN2B antagonism could be the balance between excitation and inhibition.

In the context of Down syndrome, our *in vitro* results indicate that GluN2B antagonists compensate for excessive inhibition, and could potentially be useful for acute and persistent rebalancing of synaptic function. However, despite rescuing several electrophysiological measures in hippocampal slices, we did not observe acute or lasting improvement of cognitive deficits after Ro25 treatment in Ts65Dn mice with the doses/treatment regimens used. Thus, disinhibition of a subpopulation of interneurons would appear less powerful in rescuing cognitive functions than blocking all $GABA_A$Rs, which has been shown to rescue Ts65Dn mouse memory deficits (Fernandez *et al*, 2007; Rueda *et al*, 2008). Nonetheless, although other approaches to manipulating inhibition may be more likely of benefit in Down syndrome, potential benefits of the circuit impacts of GluN2B antagonists bear further analysis in the context of other neurological diseases, including Alzheimer's disease that could involve altered inhibition (see Supplementary Discussion SI). In addition, in considering therapeutic application of GluN2B antagonists, impacts on circuit function must be considered alongside possible neuroprotective benefits.

In general, future studies will need to explore functions in not only excitatory neurons, but also in inhibitory interneurons and at the level of circuit function, to understand the diverse subunit-dependent contributions of NMDARs to normal physiological functions, as well as the potential benefits of their selective modulation in treating specific neurological diseases.

ACKNOWLEDGEMENTS

We thank Hilda Solanoy and Han Lin for injections, Shannon Powell for mouse breeding, Anna Pham for genotyping, Po-Chang Chiang for formulations, Xingrong Liu for pharmacokinetic analysis, and Jacob Schwartz for chemical synthesis.

DISCLOSURE

While conducting this study, all authors were paid employees of Genentech, a member of the Roche Group, except for Dr Shamloo who was an employee of the Stanford Behavioral and Functional Neuroscience Laboratory. The work done in this study was funded by a research contract with Genentech. Dr Weber declares that within the past 3 years he was an employee of UCSD Medical School.

REFERENCES

Bracci E, Vreugdenhil M, Hack SP, Jefferys JG (1999). On the synchronizing mechanisms of tetanically induced hippocampal oscillations. *J Neurosci* **19**: 8104–8113.

Braudeau J, Delatour B, Duchon A, Lopes-Pereira P, Dauphinot L, de Chaumont F *et al* (2011). Specific targeting of the GABA-A receptor {alpha}5 subtype by a selective inverse agonist restores cognitive deficits in Down syndrome mice. *J Psychopharmacol* **25**: 1030–1042.

Calon F, Rajput AH, Hornykiewicz O, Bedard PJ, Di Paolo T (2003). Levodopa-induced motor complications are associated with alterations of glutamate receptors in Parkinson's disease. *Neurobiol Dis* **14**: 404–416.

Chakrabarti L, Best TK, Cramer NP, Carney RS, Isaac JT, Galdzicki Z *et al* (2010). Olig1 and Olig2 triplication causes developmental brain defects in Down syndrome. *Nat Neurosci* **13**: 927–934.

Chamberland S, Topolnik L (2012). Inhibitory control of hippocampal inhibitory neurons. *Frontiers Neurosci* **6**: 165.

Chazot PL (2004). The NMDA receptor NR2B subunit: a valid therapeutic target for multiple CNS pathologies. *Curr Med Chem* **11**: 389–396.

Costa AC, Grybko MJ (2005). Deficits in hippocampal CA1 LTP induced by TBS but not HFS in the Ts65Dn mouse: a model of Down syndrome. *Neurosci Lett* **382**: 317–322.

Costa AC, Stasko MR, Schmidt C, Davisson MT (2010). Behavioral validation of the Ts65Dn mouse model for Down syndrome of a genetic background free of the retinal degeneration mutation Pde6b(rd1). *Behav Brain Res* **206**: 52–62.

Fernandez F, Morishita W, Zuniga E, Nguyen J, Blank M, Malenka RC *et al* (2007). Pharmacotherapy for cognitive impairment in a mouse model of Down syndrome. *Nat Neurosci* **10**: 411–413.

Fischer G, Mutel V, Trube G, Malherbe P, Kew JN, Mohacsi E *et al* (1997). Ro 25-6981, a highly potent and selective blocker of N-methyl-D-aspartate receptors containing the NR2B subunit. Characterization in vitro. *J Pharmacol Exper Ther* **283**: 1285–1292.

Harris AZ, Pettit DL (2007). Extrasynaptic and synaptic NMDA receptors form stable and uniform pools in rat hippocampal slices. *J Physiol* **584**(Pt 2): 509–519.

Kaufman AM, Milnerwood AJ, Sepers MD, Coquinco A, She K, Wang L *et al* (2012). Opposing roles of synaptic and extrasynaptic NMDA receptor signaling in cocultured striatal and cortical neurons. *J Neurosci* **32**: 3992–4003.

Keiser MJ, Setola V, Irwin JJ, Laggner C, Abbas AI, Hufeisen SJ *et al* (2009). Predicting new molecular targets for known drugs. *Nature* **462**: 175–181.

Kleschevnikov AM, Belichenko PV, Gall J, George L, Nosheny R, Maloney MT *et al* (2012). Increased efficiency of the GABAA and GABAB receptor-mediated neurotransmission in the Ts65Dn mouse model of Down syndrome. *Neurobiol Dis* **45**: 683–691.

Kleschevnikov AM, Belichenko PV, Villar AJ, Epstein CJ, Malenka RC, Mobley WC (2004). Hippocampal long-term potentiation suppressed by increased inhibition in the Ts65Dn mouse, a genetic model of Down syndrome. *J Neurosci* **24**: 8153–8160.

Kocsis B (2012a). Differential role of NR2A and NR2B subunits in N-methyl-D-aspartate receptor antagonist-induced aberrant cortical gamma oscillations. *Biol Psychiatry* **71**: 987–995.

Kocsis B (2012b). State-dependent increase of cortical gamma activity during REM sleep after selective blockade of NR2B subunit containing NMDA receptors. *Sleep* **35**: 1011–1016.

Lei S, McBain CJ (2002). Distinct NMDA receptors provide differential modes of transmission at mossy fiber-interneuron synapses. *Neuron* **33**: 921–933.

Liu Y, Wong TP, Aarts M, Rooyakkers A, Liu L, Lai TW *et al* (2007). NMDA receptor subunits have differential roles in mediating excitotoxic neuronal death both in vitro and in vivo. *J Neurosci* **27**: 2846–2857.

Maccaferri G, Dingledine R (2002). Control of feedforward dendritic inhibition by NMDA receptor-dependent spike timing in hippocampal interneurons. *J Neurosci* **22**: 5462–5472.

Mathur P, Graybeal C, Feyder M, Davis MI, Holmes A (2009). Fear memory impairing effects of systemic treatment with the NMDA NR2B subunit antagonist, Ro 25-6981, in mice: attenuation with ageing. *Pharmacol Biochem Behav* **91**: 453–460.

McNally JM, McCarley RW, McKenna JT, Yanagawa Y, Brown RE (2011). Complex receptor mediation of acute ketamine applica-

tion on in vitro gamma oscillations in mouse prefrontal cortex: modeling gamma band oscillation abnormalities in schizophrenia. *Neuroscience* **199**: 51–63.
Milnerwood AJ, Gladding CM, Pouladi MA, Kaufman AM, Hines RM, Boyd JD *et al* (2010). Early increase in extrasynaptic NMDA receptor signaling and expression contributes to phenotype onset in Huntington's disease mice. *Neuron* **65**: 178–190.
Mony L, Kew JN, Gunthorpe MJ, Paoletti P (2009). Allosteric modulators of NR2B-containing NMDA receptors: molecular mechanisms and therapeutic potential. *Br J Pharmacol* **157**: 1301–1317.
Okamoto S, Pouladi MA, Talantova M, Yao D, Xia P, Ehrnhoefer DE *et al* (2009). Balance between synaptic versus extrasynaptic NMDA receptor activity influences inclusions and neurotoxicity of mutant huntingtin. *Nat Med* **15**: 1407–1413.
Papouin T, Ladepeche L, Ruel J, Sacchi S, Labasque M, Hanini M *et al* (2012). Synaptic and extrasynaptic NMDA receptors are gated by different endogenous coagonists. *Cell* **150**: 633–646.
Perez-Cremades D, Hernandez S, Blasco-Ibanez JM, Crespo C, Nacher J, Varea E (2010). Alteration of inhibitory circuits in the somatosensory cortex of Ts65Dn mice, a model for Down's syndrome. *J Neural Transm* **117**: 445–455.
Porter JT, Cauli B, Staiger JF, Lambolez B, Rossier J, Audinat E (1998). Properties of bipolar VIPergic interneurons and their excitation by pyramidal neurons in the rat neocortex. *Eur J Neurosci* **10**: 3617–3628.
Rueda N, Florez J, Martinez-Cue C (2008). Chronic pentylenetetrazole but not donepezil treatment rescues spatial cognition in Ts65Dn mice, a model for Down syndrome. *Neurosci Lett* **433**: 22–27.
Sohal VS, Zhang F, Yizhar O, Deisseroth K (2009). Parvalbumin neurons and gamma rhythms enhance cortical circuit performance. *Nature* **459**: 698–702.
Tamamaki N, Yanagawa Y, Tomioka R, Miyazaki J, Obata K, Kaneko T (2003). Green fluorescent protein expression and colocalization with calretinin, parvalbumin, and somatostatin in the GAD67-GFP knock-in mouse. *J Comp Neurol* **467**: 60–79.
Tovar KR, Westbrook GL (1999). The incorporation of NMDA receptors with a distinct subunit composition at nascent hippocampal synapses in vitro. *J Neurosci* **19**: 4180–4188.
Vida I, Halasy K, Szinyei C, Somogyi P, Buhl EH (1998). Unitary IPSPs evoked by interneurons at the stratum radiatum-stratum lacunosum-moleculare border in the CA1 area of the rat hippocampus in vitro. *J Physiol* **506**(Pt 3): 755–773.
von Engelhardt J, Doganci B, Jensen V, Hvalby O, Gongrich C, Taylor A *et al* (2008). Contribution of hippocampal and extrahippocampal NR2B-containing NMDA receptors to performance on spatial learning tasks. *Neuron* **60**: 846–860.
Vreugdenhil M, Bracci E, Jefferys JG (2005). Layer-specific pyramidal cell oscillations evoked by tetanic stimulation in the rat hippocampal area CA1 in vitro and in vivo. *J Physiol* **562**(Pt 1): 149–164.
Wang HX, Gao WJ (2009). Cell type-specific development of NMDA receptors in the interneurons of rat prefrontal cortex. *Neuropsychopharmacology* **34**: 2028–2040.
Watanabe M, Inoue Y, Sakimura K, Mishina M (1993). Distinct distributions of five N-methyl-D-aspartate receptor channel subunit mRNAs in the forebrain. *J Comp Neurol* **338**: 377–390.
Wessell RH, Ahmed SM, Menniti FS, Dunbar GL, Chase TN, Oh JD (2004). NR2B selective NMDA receptor antagonist CP-101,606 prevents levodopa-induced motor response alterations in hemiparkinsonian rats. *Neuropharmacology* **47**: 184–194.

This work is licensed under a Creative Commons Attribution-NonCommercial-NoDerivs 3.0 Unported License. To view a copy of this license, visit http://creativecommons.org/licenses/by-nc-nd/3.0/

Supplementary Information accompanies the paper on the Neuropsychopharmacology website (http://www.nature.com/npp)